



Saturation model for secondary electron multiplier detectors

P.M. Shikhaliev¹

A.F. Ioffe Physical-Technical Institute, Politekhnicheskaya 26, 194021, St. Petersburg, Russia

Received 25 August 1997; received in revised form 18 May 1998

Abstract

An analytical saturation model for secondary electron multiplier detectors (SEM) has been developed. This model describes SEM detector operation at high output currents when the significant part of the conduction current of dynodes passes to the electron avalanche current and the dynode potential is nonuniformly redistributed. The following main parameters of the SEM detectors in the saturated mode are predicted: the output current, conduction current and gain depending on input current, the potential, electric field and electron avalanche current distribution along the dynode system. A novel type of the SEM with nonlinear dynode resistance (SEM-NDR) that provides an extended dynamic range is suggested. The model predictions are in good agreement with the experimental results. The samples of the SEM-NDR have also been developed and investigated. © 1999 Elsevier Science B.V. All rights reserved.

1. Introduction

Saturation effects have a very important influence on the operation of secondary electron multiplier (SEM) detectors. There are three types of saturation effects that are described in the literature. First is space charge saturation, which arises due to the decrease of the interdynode electric field by the space charge of the electron avalanche [1–3]. The second type of saturation arises when the positive wall charge which is generated soon after the electron avalanche neutralizes the dynode electric field of the SEM [4]. The first type of saturation is important for single channel electron multipliers that have a high gain and large channel diameter [5], while the second type is important for the microchannel plates (MCP) with the straight chan-

nels [1,4]. Both types of saturation can also influence the operation of the discrete dynode SEM, when the input of the detector is irradiated by very short and high intensity pulses of particles [6]. Theoretical models for space and wall charge saturation are described in a number of works and are in good agreement with the experimental results [4,7,8]. Space and wall charge saturation are observed in the pulse operation mode of the detectors, when the average frequency of the output pulses is not high and the gain of the detector is completely recovered between two pulses. However, when the average frequency of the output pulses is high, the gain of the detector cannot recover between two pulses and a third type of the saturation (so-called current saturation) arises [1,9]. In this case, a significant part of the conduction current of dynodes passes to the electron avalanche current (especially in the end parts of the dynode system) and the dynode potential and the interdynode electric fields

¹ E-mail: peter@fields.ioffe.rssi.ru.

are nonuniformly redistributed along the dynode system. Though the current saturation mechanism is universal for all types of SEM detectors, most works are devoted to the investigation of MCP detectors because MCPs are strongly influenced by current saturation effect due to the small conduction current of the channel on the one hand, and the continuous expansion of the application field of the MCP detectors on the other hand.

Different approaches have been used for the analytical description of the current saturation mode of the MCP detectors. The MCP channels have been presented as consecutively connected RC chains whose parameters were found by numerical solution of the corresponding Kirchoff equations [10]. The microscopic structure of the electric field inside the channels were also considered in some works [11,12]. Simple analytical models of MCP operation were suggested by many authors using, however, empirical dependencies that were found experimentally [9,13–19]. Finally, probabilistic models, where the MCP channels were presented as paralyzable and nonparalyzable photon counters have been developed [20–22]. Though the current saturation of SEM detectors has been investigated in many works, a model that should satisfactorily predict the main SEM parameters in the saturated mode is not available [9,23]. The main impediment for the development of such a model is the difficulty of describing the electron avalanche behaviour in the nonuniform electric field of the dynodes because the parameters of the electron avalanche depend on the dynode electric field redistribution, but at the same time this redistribution arises due to the electron avalanche current. In the present work a generalized analytical model of current saturation for SEM detectors has been developed. Our model predicts the following main parameters of the SEM in the saturated mode: the potential and electric field distribution along the dynode system, the electron avalanche current distribution, the output current, conduction current and gain depending on input current. A novel type of SEM with nonlinear dynode resistance (SEM-NDR) that provides an extended dynamic range has been suggested. The predictions of the model are in good agreement with the experimental results. The samples of the SEM-NDR have also been developed and investigated.

2. Theory

2.1. Saturation model

Consider a SEM with a continuous dynode system. It may be a single channel electron multiplier (CEM) or MCP. As will be shown below, the results to be found for the continuous dynode SEM are also correct for the discrete dynode SEM. Let L , R_0 and C be the length, resistance and capacitance of the channel of the SEM (Fig. 1a). In the unsaturated mode, when the average frequency of the output pulses is less than $1/R_0C$, where R_0C is the time constant of the channel, the electron number and the average electron current in the channel are given by the well-known exponential law [1]:

$$K(x) = K_0^{x/L} = e^{(x/L) \ln K_0}, \tag{1a}$$

$$i(x) = i_0 K(x) = i_0 K_0^{x/L}, \tag{1b}$$

where, $K(x)$ is the number of avalanche electrons at a distance x from the channel beginning in the single electron operation mode, K_0 the gain of the SEM, $i(x)$ the average electron current at the point of x , i_0 the average input current of the detector. The detector gain K_0 depends on the voltage

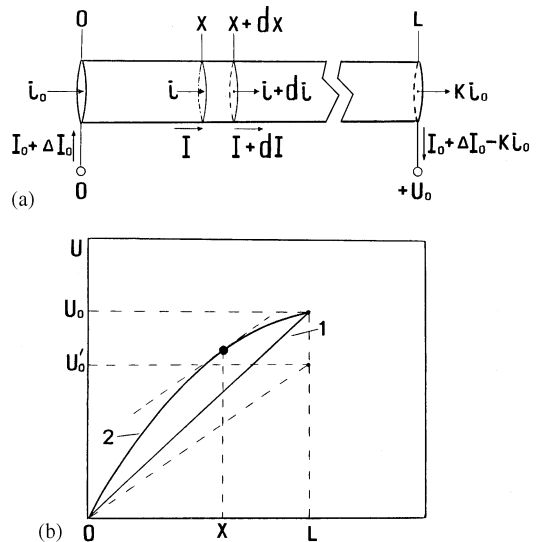


Fig. 1. Diagram of the continual channel SEM (a) and the potential distribution along the channel (b), for unsaturated (1) and saturated (2) modes.

U_0 applied along the channel as

$$\ln K_0 = F(U_0), \quad (2)$$

where the function $F(U_0)$ may be determined experimentally and approximated analytically. The output and conduction currents of the detector are determined as $i(L) = i_0 K_0$ and $I_0 = U_0/R_0$. The potential and electric field distributions along the channel in the unsaturated mode are $U(x) = U_0(x/L)$ and $E(x) = E_0 = U_0/L$, and the condition $i_0 K_0 \ll I_0$ is realized.

When the output pulse frequency is increased, the average output current is also increased and the average conduction current is decreased in the end parts of the channel because significant part of this current passes to avalanche current. Since the electric field of a dynode is formed by the conduction current, so this field is also decreased in the end part of the channel. The decrease of the potential and electric field in the end part of the channel leads to their increase in the beginning parts of the channel. Thus, the nonuniform redistribution of the dynode potential and electric field arises. The exponential laws 1(a) and (b) for the electron avalanche and average electron current become incorrect in a nonuniform electric field, the detector gain depends on output current, and is decreased when the output current is increased.

As the input current i_0 is given to SEM, the conduction current I_0 is increased by ΔI_0 and the condition

$$I(x) + i(x) = I(0) + i(0) = I_0 + \Delta I_0 + i_0 \quad (3)$$

must be realized for any point x of the channel. Since $I(x) = dU(x)/dR$ and $R(x) = R_0 x/L$, then

$$I(x) = \frac{L}{R_0} \frac{dU(x)}{dx} \quad (4)$$

and the condition (3) may be rewritten in the form

$$\frac{L}{R_0} \frac{dU(x)}{dx} + i(x) = I_0 + \Delta I_0 + i_0. \quad (5)$$

Consider the element dx of the channel in which the gain $K(x)$ may be believed to be constant. The avalanche current may be written:

$$di(x) = (di/dx)dx. \quad (6)$$

In the unsaturated mode di/dx may easily be derived from Eq. (1b) as

$$di/dx = \frac{\ln K_0}{L} dx. \quad (7)$$

However, the expression (1b) is incorrect for the saturated mode and the expression (7) cannot be used directly. To overcome this difficulty we use the following method. The potential distribution along the channel in the saturated and unsaturated mode is shown in Fig. 1b. The exact shape of the potential distribution in the saturated mode is unknown, but it was considered in Fig. 1b that in this mode the electric field (i.e., dU/dx) in the end part of the channel is lower than that of in the beginning parts. It may be seen from Fig. 1b that the gain $K(x)$ at the point of x in the saturated mode is the same as that in the unsaturated mode, if in the latter case the applied voltage is equal to $U'_0 = L dU/dx$, and the gain K'_0 is determined as $\ln K'_0 = F(U'_0) = F(L dU/dx)$. Thus, the expression (7) may be used for the saturated mode if $\ln K_0$ is substituted by $\ln K'_0$. Taking into account these considerations expression (6) may be presented as $di(x) = (1/L) F(L(dU/x))i(x)dx$ and considering Eq. (5) we find

$$\frac{di}{dx} = \frac{1}{L} i F\left(L \frac{dU}{dx}\right),$$

$$\frac{L}{R_0} \frac{dU}{dx} + i = I_0 + \Delta I_0 + i_0 \quad (8)$$

with initial conditions

$$i(0) = i_0, \quad i(L) = Ki_0, \quad U(0) = 0, \quad U(L) = U_0. \quad (9)$$

The solution of the system (8) taking into account Eq. (9) gives the potential and electric field distributions $U(x)$ and $E(x) = dU/dx$ along the channel for the different input currents i_0 , as well as the gain K , the output current Ki_0 and the conduction current $I_0 + \Delta I_0$ depending on input current i_0 . All these dependencies are found analytically for the first time. The function $F(U_0)$ may be found experimentally but an analytical expression for it is required to integrate the system (8). Measured curves and some analytical approximations for $F(U_0)$ are presented in Fig. 2. To restore the analytical expressions for $F(U_0)$ different approximations may be used. The expressions $F(U_0) = (a \ln b U_0)/U_0$

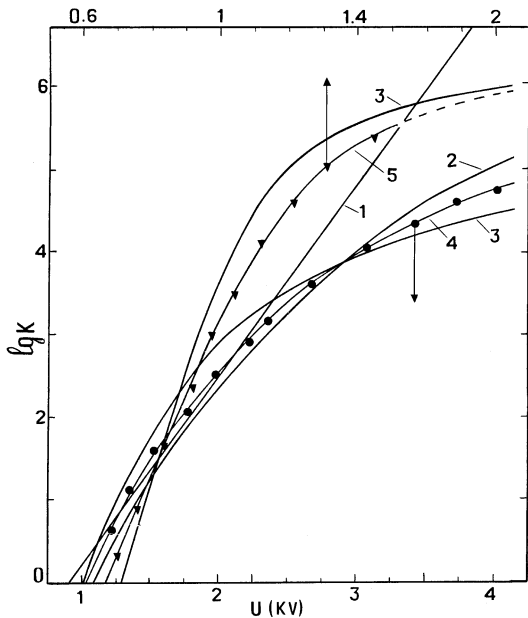


Fig. 2. Linear (1), parabolic (2) and hyperbolic (3) approximations of the function $F(U_0) = \ln K(U_0)$ and the experimental curves for the discrete dynode (VEU-1) (4) and MCP (channel diameter – $18 \mu\text{m}$ channel length-to-diameter ratio – 70) (5) detectors. The detectors have been tested in a current operation mode with a beam of 5 keV H_2^+ ions.

and $F(U_0) = aU_0^{1/3} \ln bU_0$ were found for the straight and curved channel electron multipliers, respectively [24]. The approximation $F(U_0) = a \ln bU_0 - cU_0$ may be used for the discrete dynode SEM [25]. The parabolic $F(U_0) = a(b + U_0)(c - U_0)$ and hyperbolic $F(U_0) = a(1 - b/U_0)$ approximations may also be used. In the present work we use the linear function $F(U_0) = a(U_0 - b)$ [25] as a zeroth approximation and the hyperbolic function $F(U_0) = a(1 - b/U_0)$ to find more precise results. Evidently, the constants a, b and c that are included in the expressions for $F(U_0)$ must be determined separately in every case.

2.2. “Ideal” detector model

The system (8) of the differential equations with the linearly approximated function $F(U_0)$ is

$$\frac{di}{dx} = \frac{1}{L} \frac{\ln K_0}{U_0 - U_{\min}} i \left(L \frac{dU}{dx} - U_{\min} \right),$$

$$\frac{L}{R_0} \frac{dU}{dx} + i = I_0 + \Delta I_0 + i_0,$$

where $F(U_0) = \ln K_0$, $F(U_{\min}) = 0$. The relative values of U, i and x will be used in further considerations: $V = U/U_0, j = i/I_0, z = x/L$. Then

$$\frac{dj}{dz} = bj \left(\frac{dV}{dz} - 1 + \beta \right),$$

$$\frac{dV}{dz} + j = 1 + \alpha + j_0 \tag{10}$$

with initial conditions $j(0) = j_0, j(1) = Kj_0, V(0) = 0, V(1) = 1$, where $\alpha = \Delta I_0/I_0, j_0 = i_0/I_0, \beta = 1 - V_{\min}, b = \ln K_0/\beta$. Using the relative values of U, i and x we can provide universality to the system (10) because in such a form this system includes only three relative parameters α, β and b that depend on the type of the detector.

Considering the second equation of the system (10) in the first we find

$$\frac{dj}{dz} = bj(\alpha + \beta + j_0 - j).$$

The integration of this equation taking into account the condition $j(0) = j_0$ gives

$$j(z) = \frac{\alpha + \beta + j_0}{1 + [(\alpha + \beta)/j_0] e^{-b(\alpha + \beta + j_0)z}}. \tag{11}$$

Taking into account $b = \ln K_0/\beta$, the expression (11) may be presented in the form

$$j(z) = \frac{\alpha + \beta}{\alpha + \beta + j_0 K_0^{(1 + \alpha/\beta)z}} j_0 K_0^{(1 + \alpha/\beta)z}. \tag{11a}$$

In the unsaturated mode $\alpha \ll \beta$ and $j_0 K_0^{(1 + \alpha/\beta)z} \ll \beta$. Then Eq. (11a) takes the well-known form $j(z) = j_0 K_0^z$, that is identical with Eq. (1b) for the unsaturated mode. The integration of the second equation of system (10) taking into account the condition $V(0) = 0$ gives

$$V(z) = (1 + \alpha + j_0)z + \frac{1}{b} \ln \frac{\alpha + \beta + j_0}{\alpha + \beta + j_0 \exp[b(\alpha + \beta + j_0)z]}. \tag{12}$$

Considering the condition $V(1) = 1$ in Eq. (12) we find

$$K_0 j_0 = (\alpha + \beta)(1 - e^{-\alpha b}). \quad (13)$$

The expression (13) gives the conduction current $1 + \alpha$ depending on input current j_0 .

The electric field distribution along the channel is

$$E(z) = \frac{dV}{dz} = 1 + \alpha + j_0 - \frac{\alpha + \beta + j_0}{1 + [(\alpha + \beta)/j_0] e^{-b(\alpha + \beta + j_0)z}}. \quad (14)$$

The detector gain K may be derived from Eq. (11) using Eq. (13) and condition $j(1) = Kj_0$. We find $K = K_0$. This is a most important result: the detector gain behavior in the saturated mode is predetermined by the form of the function $F(U_0)$. For an “ideal” detector, when the function $F(U_0)$ is linear, the detector gain is not changed for any values of the output current. It means that in the saturated mode of the “ideal” detector the decrease of the gain in the end parts of the channel is completely compensated by its increase in the beginning part of the channel. However, the function $F(U_0)$ is nonlinear for “real” detectors and is slowly increased for high U_0 (see Fig. 2). Therefore, in the saturated mode, the gain of the end part of a “real” detector is decreased more strongly than the increase of the gain of the beginning part, and the complete gain of the SEM is decreased.

Fig. 3 shows the calculated dependence of the output and conduction currents on the input current for the discrete dynode detector VEU-1 with linearly approximated $F(U_0)$ (the detector VEU-1 will be described in Section 3). As we see, the detector gain is not changed at high output currents, and the conduction current is close to the output current but these difference become constant according to Eq. (13): $1 + \alpha - K_0 j_0 \rightarrow 1 - \beta$, when $\alpha \rightarrow \infty$. It must be considered that the “ideal” detector approximation is correct for “real” detectors if the applied voltage U_0 corresponds to the quasilinear part of the dependence $F(U_0)$ for the “real” detector. Besides, the output current of such a “real” detector must be limited so that the electric field in the beginning part of the dynode system is

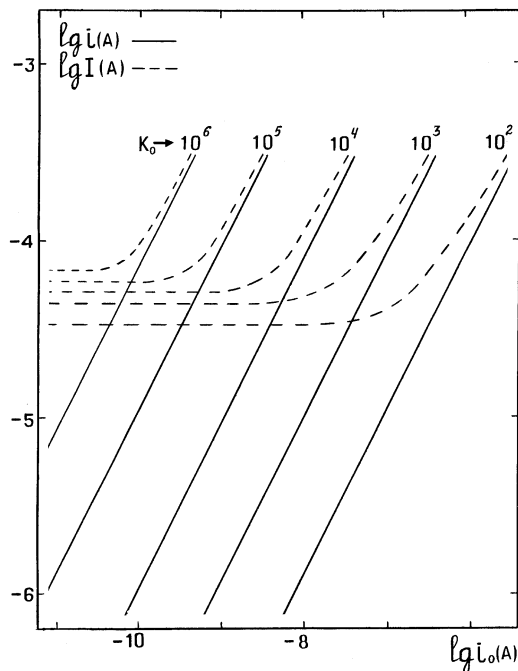


Fig. 3. Calculated conduction I and output i currents of the “ideal” detector depending on the input current for the different initial gains K_0 .

less than the critical value U_1/L , where U_1 is the critical voltage that limits the quasilinear part of the function $F(U_0)$.

2.3. “Real” detector model

As noted above, the hyperbolic approximation of the function $F(U_0)$ is in good agreement with the experimental curves $F(U_0)$ for “real” detectors. In this case

$$F(U_0) = \ln K(U_0) = \left(1 - \frac{U_{\min}}{U_0}\right) \ln K_{\max}, \quad (15)$$

where $K(U_{\max}) = K_{\max}$, $K(U_{\min}) = 1$.

The consideration of Eq. (15) in Eq. (8) gives

$$\frac{dj}{dz} = \left[1 - (1 - \beta) \left(\frac{dV}{dz}\right)^{-1}\right] \ln K_{\max},$$

$$\frac{dV}{dz} = 1 + \alpha + j_0 - j, \quad (16)$$

$$j(0) = j_0, \quad j(1) = Kj_0, \quad V(0) = 0, \quad V(1) = 1.$$

The integration of the system (16) taking into account conditions $j(0) = j_0$, and $V(0) = 0$ gives

$$\left[\frac{j}{j_0} \right]^{(1+\alpha+j_0)/(1-\beta)} = \left[1 - \frac{j-j_0}{\alpha+\beta} \right] e^{[(\alpha+\beta+j_0)/(1-\beta)]z \ln K_{\max}},$$

$$V = (1 + \alpha + j_0)z - \frac{1}{\ln K_{\max}} \left[j - j_0 - (1 - \beta) \ln \left(1 - \frac{j-j_0}{\alpha+\beta} \right) \right]. \quad (17)$$

The first equation of (17) can be presented in the form

$$j(z) = j_0 K_0^z \left[1 - \frac{j-j_0}{\alpha+\beta} \right]^{(1-\beta)/(1+\alpha+j_0)}. \quad (17a)$$

Since the conditions $j_0, j, \alpha \ll \beta$ are realized in the unsaturated mode, Eq. (17a) reduces to the well-known form (1b): $j(z) = j_0 K_0^z$. Now considering the initial conditions $j(1) = Kj_0$ and $V(1) = 1$ in the first and second equations of (17) we find:

$$\alpha \ln K_{\max} = Kj_0 - (1 - \beta) \ln \left(1 - \frac{Kj_0}{\alpha+\beta} \right),$$

$$(1 + \alpha) \ln K = Kj_0 + \ln K_0. \quad (18)$$

Solving Eq. (18) we can find the detector gain K , the output current Kj_0 and the conduction current $1 + \alpha$ depending on the input current j_0 . Considering K and α in Eq. (17) the dependencies $j(z)$, $V(z)$ and $E(z)$ may be found for different output currents. Unfortunately, Eqs. (17) and (18) cannot be solved analytically and the functions $K(j_0)$, $\alpha(j_0)$, as well as $j(z)$, $V(z)$ and $E(z)$ may be found by numerical calculations. Figs. 4 and 5 show the calculated dependencies of the output current, conduction current and gain on the input current. Note that these curves have long been established experimentally for all types of SEM detector, but have been found analytically for the first time. Figs. 6 and 7 show the potential and electric field distributions along the SEM dynode system. As it may be seen, these distributions are similar for the “ideal” and “real” detectors, but the gain of the “real” detector is decreased dramatically while the gain of the “ideal” detector is not changed. Fig. 8 shows the electron avalanche current distribution along the dynode system. As we see, when the output current is low,

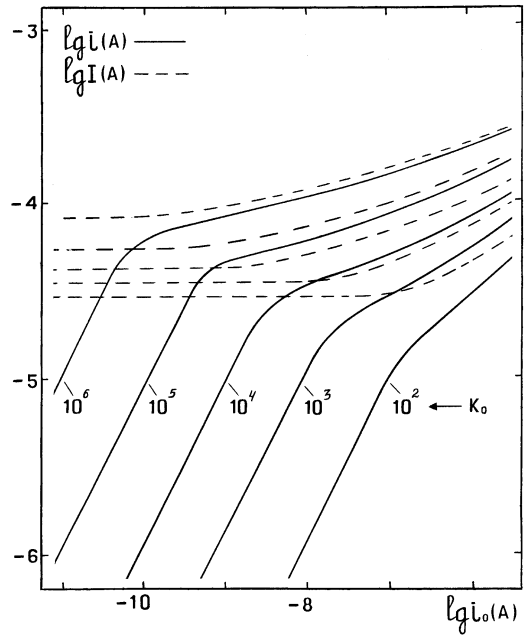


Fig. 4. Calculated conduction I and output i currents of the “real” detector depending on the input current for the different initial gains K_0 .

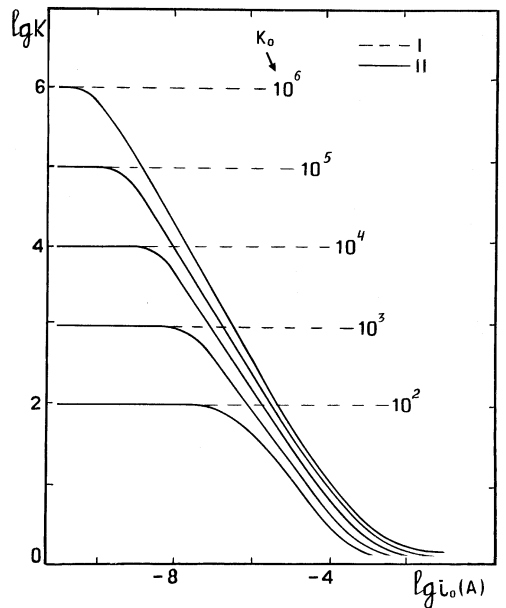


Fig. 5. Calculated gains of the “ideal” (I) and “real” (II) detectors depending on input current for the different initial gains K_0 .

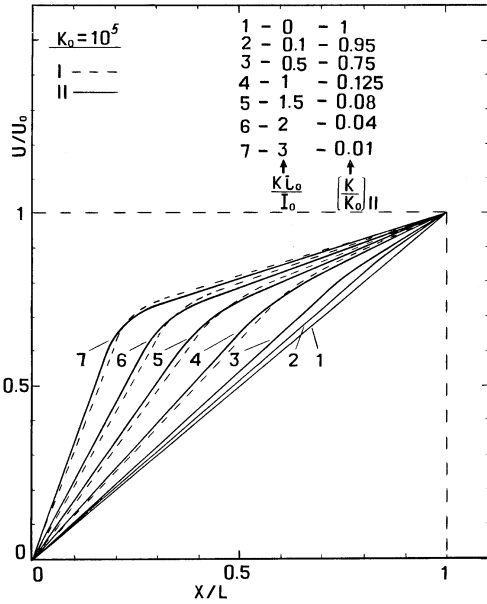


Fig. 6. Calculated potential distribution along the channel for the “ideal” (I) and “real” (II) detector at the different output currents Ki_0 .

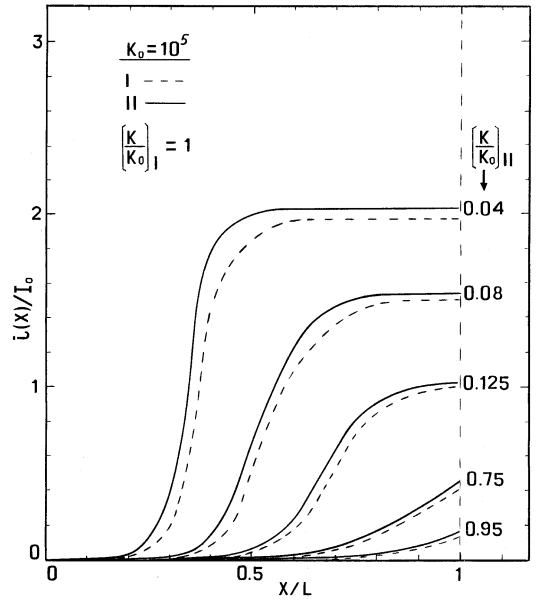


Fig. 8. Calculated electron avalanche distribution along the channel for the “ideal” (I) and “real” (II) detectors at the different output currents Ki_0 .

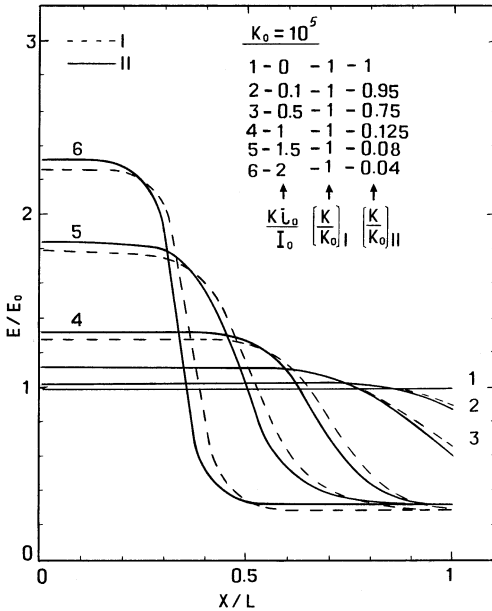


Fig. 7. Calculated electric field distribution along the channel for the “ideal” (I) and “real” (II) detectors at the different output currents Ki_0 .

the avalanche current increases exponentially according to Eq. (1b) and the gain is slightly decreased. When the output current is high, the avalanche current is increased exponentially only in the beginning parts of the dynode system and is not increased practically in the end parts due to saturation effects. It means that the electric field in the end part of the dynode system is strongly decreased and is near to critical value U_{min}/L that provides only unit gain. Note that the avalanche current distributions for “ideal” and “real” detectors are also similar for the fixed output current, but the gain of the “real” detector is strongly decreased.

2.4. SEM detector with nonlinear dynode resistance

The dynode resistance of the conventional SEM is uniformly distributed along the dynode system: $R(x) = R_0x/L$. The dynode potential and electric field distributions are also uniform in the unsaturated mode. In the saturated mode, however, the dynode potential and dynode electric field are nonuniformly redistributed, as is shown in Figs. 6

and 7. Now consider a SEM with ununiformly distributed dynode resistance. Let the dynode resistance be increased in the end part of the channel more strongly than the linear law, and

$$R(x) = R_0 f(x), \tag{19}$$

where $f(0) = 0, f(1) = 1$. Then the electric field of the dynode in the end part is higher than that in the beginning part. Assume that the function $f(x)$ is such that the electric field distribution in the unsaturated mode is as shown in Fig. 9a, position 1. As the output current is increased and saturation arises, the distribution 1 continuously passes to 2 which is identical with the electric field distribution of the conventional SEM in the unsaturated mode. When the output current is increased more, the electric field distribution continuously passes from position 2 to 3, which is identical with the distribution of the conventional SEM in the saturated mode (see Fig. 7). Thus, the saturation of the SEM-NDR (i.e. passage 1 → 3) arises at an output current that is many times higher than the saturation currents of the conventional SEM (passage 2 → 3). The equation that describes SEM-NDR operation may be found from Eq. (10)

considering Eq. (19):

$$\frac{dj}{dz} = jF \left(U_0 \frac{dV}{dz} \right),$$

$$\frac{dV}{dz} \left(\frac{df}{dz} \right)^{-1} + j = 1 + \alpha + j_0 \tag{20}$$

under additional conditions $f(0) = 0, f(1) = 1$.

Evidently, this system cannot be solved in the general form and the function $f(z)$ must be predetermined analytically. The solution of the system (20) for different types of the function $f(z)$ gives the optimized resistance distribution that provides the maximum dynamic range of the SEM-NDR. Fig. 9a shows that the optimal choice of the function $f(z)$ is important because if the resistance of the end part of the channel is too high, the electric field in this part becomes more than the critical value U_1/L . In this case the inverse nonlinearity effect may arise, i.e. the gain of the saturated SEM-NDR may be more than that of the unsaturated SEM-NDR. It must be noted that the MCPs with the nonlinear channel resistance have recently been considered in Refs. [23,26], but an operation model for such MCPs, as well as for the conventional SEM was not available. The first test results of MCP-NDR showed (the resistance of the end part of MCP channel was ~ 10 times more than that of the beginning part, but the resistance distribution $f(x)$ along the channel was unknown) that such MCPs have a high gain at the high output currents (saturated mode), at which the gain of the conventional MCPs is strongly decreased [23]. However, the results for the low output current mode (unsaturated mode) of MCP-NDR are not presented in Ref. [23]. According to our theory, the inverse nonlinearity effect may arise for the resistance relation 1:10 of the beginning and end part of the channel and the gain of such MCP-NDR may be low in the unsaturated mode.

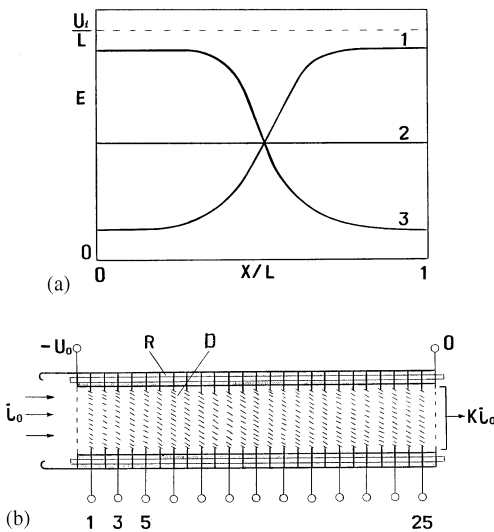


Fig. 9. Electric field distribution along the SEM-NDR channel (a) and the diagram of the VEU-1 (b): R – resistive ring, D – dynode.

3. Experimental results

Discrete dynode models of the SEM are routinely used for the development of the theory of continuous dynode SEM. It is assumed that the

channel of the SEM consists of a number of consecutively placed discrete dynode, whose number depends on the length-to-diameter relation of the channel. The parameters of such discrete dynode SEM are easily calculated and the results are in good agreement with the experimental results for the continual dynode SEM. In the present work we have developed the saturation theory of the SEM using the continuous dynode model, but the discrete dynode SEM has been used for the experimental testing of the theory. As will be shown below, the predictions of the theory are in good agreement with the experimental results for both continuous and discrete dynode SEM. A commercial discrete dynode jalousie type multiplier VEU-1 with aluminium dynodes has been used in our experiments (Fig. 9b). The dynode number is 25 [5,27]. The dynode resistance of this detector consists of small resistive rings that are placed between dynodes. These rings are cut from the lead glass tube, reduced in the hydrogen atmosphere and have a surface resistivity that is identical to the resistivity of the channel electron multipliers. The resistance of every ring is equal to $2.4\text{ M}\Omega$, and the complete resistance of the dynode system is $30\text{ M}\Omega$. VEU-1 was placed in the mass-spectrometer MI-1201 and was tested in a current operation mode with a beam of 5 keV H_2^+ ions. The ion beam current was measured with high precision Faraday cups. The ion current was controlled by changing the emission current of the ion source [28]. The output current of VEU-1 was measured with a microammeter. The dynode potentials were measured with a voltmeter at special contacts which are connected to dynodes 1, 3, 5, ..., 25. The input resistance of the voltmeter was many times higher than the interdynode resistance and could not influence the value of the latter. Figs. 10 and 11 show the measured distribution of the potential and electric field along the dynode system for the different values of the output current. The comparison of these curves with Figs. 6 and 7 shows that the model predictions are in good agreement with the experimental results. We could change the dynode resistivity of the detector by substitution of the resistive rings to provide SEM-NDR. However, we could provide only step up dynode resistivity (but a quasicontinuously changing resistivity is desirable) because the resistive

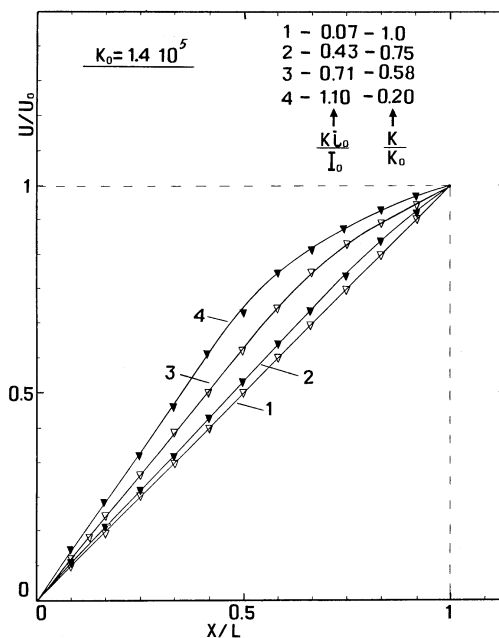


Fig. 10. Measured potential distribution along the dynode system of the detector VEU-1 at the different output currents Ki_0 .

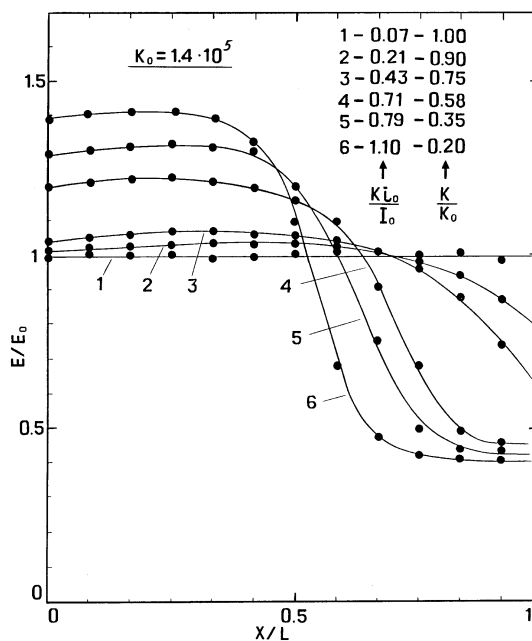


Fig. 11. Measured electric field distribution along the dynode system of the detector VEU-1 at the different output currents Ki_0 .

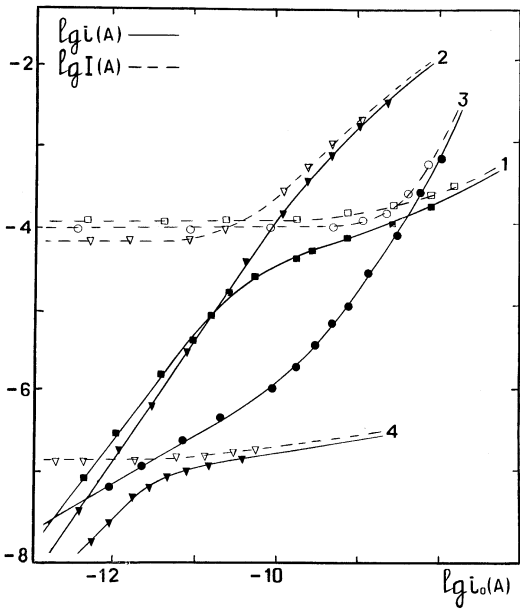


Fig. 12. Measured conduction (I) and output (II) currents depending on the input current for the conventional SEM (1), first (2) and second (3) SEM-NDR, and bare MCP detector (4).

rings with the optimal parameters were not available. The resistances of the rings between dynodes 1–8, 9–16 and 17–25 were R , R and $2R$ for the first SEM-NDR and $0.5R$, R and $2R$ for the second SEM-NDR, respectively. The output current, conduction current and gain of VEU-1 were measured for the conventional and nonlinear dynode resistance distributions. Figs. 12 and 13 show that the resistance distribution of the first SEM-NDR provides a significant extension of the dynamic range, while the second distribution leads to an inverse nonlinearity effect and the gain of such an SEM-NDR in the saturated mode is higher than in the unsaturated mode.

We also studied the saturation characteristics of a bare MCP. This experiment was described earlier in detail [28] and we present only some curves in Figs. 12 and 13. Note that, similar curves for the MCP detectors were found in many works and are in good agreement with the model predictions.

4. Conclusions

The described saturation model may be used for all types of the SEM detectors with continuous and discrete dynode systems, as well as for photomultipliers and it is useful to point out the following.

Although the function $F(U_0)$ must be known a priori before the saturation properties can be estimated, this function can easily be restored by the computer fitting using the experimental dependence $K(U_0)$ for unsaturated mode, and the system (8) can be numerically integrated.

The solution of this system gives the main parameters of the SEM detectors in the saturated mode that extends the dynamic range of these detectors.

Second, the dynode resistivity distribution function $f(x)$ may be optimized by the testing of the different types of $f(x)$. It allows the development of a novel SEM-NDR, particularly the MCP-NDR with the strongly extended dynamic range.

Finally, the predicted channel potential distribution function may be used to study the “adjacency effect” of the MCP channels [22,28] that was observed experimentally in [29] for the first time but was not modelled and studied theoretically.

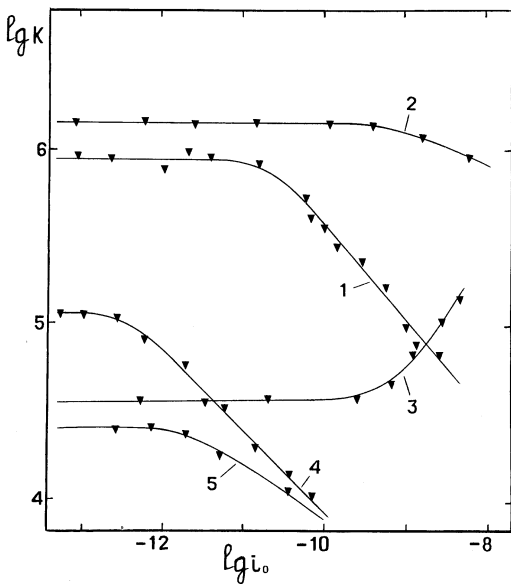


Fig. 13. Measured detector gain depending on input current for the conventional SEM (1), first (2) and second (3) SEM-NDR, and bare MCP detector (4,5).

References

- [1] C. Loty, *Acta Electronica* 14 (1) (1971) 107.
- [2] J.L. Wiza, *Nucl. Instr. and Meth.* 162 (1979) 587.
- [3] G.W. Fraser et al., *Nucl. Instr. and Meth. A* 291 (1990) 595.
- [4] G.W. Fraser, *IEEE Trans. Nucl. Sci.* NS-30 (1983) 455.
- [5] M.R. Ainbund, B.V. Polenov, *Open-Type Secondary-Electron Multipliers and their Applications*, Energoizdat, Moscow, 1981 (in Russian).
- [6] K. Siegbahn, *Alpha-, Beta- and Gamma-Ray Spectroscopy*, North-Holland, Amsterdam, 1966.
- [7] W. Baumgartner, J. Schmidt, *J. Phys. D* 5 (1972) 1769.
- [8] W. Baumgartner, B. Gillard, *Adv. Electron. Electron Phys.* A 40 (1972) 113.
- [9] G.W. Fraser, M.T. Pain, J.E. Lees, J.F. Pearson, *Nucl. Instr. and Meth. A* 306 (1991) 247.
- [10] M. Bassan, L. Giudicotti, R. Pasqualotto, A. Sardella, *SPIE* 2006 (1993) 170.
- [11] E. Gatti, K. Oba, P. Rehak, *IEEE Trans. Nucl. Sci.* NS-30 (1983) 461.
- [12] D.C. Anacker, J.L. Erskine, *Rev. Sci. Instr.* 62 (1991) 1246.
- [13] D.B. Soul, *Nucl. Instr. and Meth.* 97 (1971) 555.
- [14] B.A. Jacoby, D.E. Kotecki, R.D. Lear, *IEEE Trans. Nucl. Sci.* NS-30 (1983) 4674.
- [15] E.H. Eberhardt, *IEEE Trans. Nucl. Sci.* NS-28 (1981) 712.
- [16] M. Liptak, W.G. Sandie, E.G. Shelley, D.A. Simpson, H. Rosembauer, *IEEE Trans. Nucl. Sci.* NS-31 (1984) 780.
- [17] W.B. Feller, *SPIE* 1243 (1990) 149.
- [18] R.Y. Levine, M. Zatet, *Rev. Sci. Instr.* 62 (1991) 2602.
- [19] G.W. Fraser, M.T. Pain, J.E. Lees, *Nucl. Instr. and Meth. A* 327 (1993) 328.
- [20] D.J. Cho, G.M. Morris, *SPIE* 976 (1988) 172.
- [21] A. Sharma, J.G. Walker, *Quantum Opt.* 1 (1989) 11.
- [22] A. Sharma, J.G. Walker, *Rev. Sci. Instr.* 83 (1992) 5784.
- [23] N.M. Shyutte, E.A. Platov, V.I. Beloglasov et al., *Instr. Expt. Techn.* 4 (1995) 102.
- [24] G. Eschard, B.W. Manley, *Acta Electronica* 14 (1) (1971) 33.
- [25] A.G. Berkovski, V.A. Gavanin, I.N. Zaidel, *Vacuum Photoelectric Devices*, Energiya, Moscow, 1988 (in Russian).
- [26] E.V. Plujnikova, N.F. Lebedev, V.I. Beloglasov et al., *Patent N1828330*, Russian Federation, 1993.
- [27] M.R. Ainbund, N.V. Dunaevskaya, B.A. Mamyurin, B.N. Shustrov, *Electronnaya Tekhnica, Ser. 4* (4) (1968) 45.
- [28] P.M. Shikhaliev, *Instr. Expt. Tech.* 2 (1997) 81.
- [29] N.M. Shyutte, S.M. Sheronova, G.P. Vasnina, E.A. Platov, V.G. Kaptsov, *Instr. Expt. Tech.* 1 (1987) 175.